

## Rates of basin-wide rockwall retreat in the K2 region of the Central Karakoram defined by terrestrial cosmogenic nuclide $^{10}\text{Be}$

Yeong Bae Seong <sup>a,b,\*</sup>, Lewis A. Owen <sup>a</sup>, Marc W. Caffee <sup>c</sup>, Ulrich Kamp <sup>d</sup>, Michael P. Bishop <sup>e</sup>, Andrew Bush <sup>f</sup>, Luke Copland <sup>g</sup>, John F. Shroder <sup>e</sup>

<sup>a</sup> Department of Geology, University of Cincinnati, P.O. Box 0013, Cincinnati, OH 45221-0013, USA

<sup>b</sup> Department of Earth and Environmental Sciences, Korea University, Seoul, 136-704, South Korea

<sup>c</sup> Dept of Physics/PRIME Laboratory, Purdue University, West Lafayette, IN 47906, USA

<sup>d</sup> Department of Geography, The University of Montana, Missoula, MT 59812-5040, USA

<sup>e</sup> Department of Geography and Geology, University of Nebraska—Omaha, 6001 Dodge Street, Omaha, NE 68182-0199, USA

<sup>f</sup> Department of Earth and Atmospheric Sciences, University of Alberta, 1-26 Earth Sciences Building, Edmonton, Alberta, Canada T6G 2E3

<sup>g</sup> Department of Geography, University of Ottawa, Ottawa, Ontario, Canada K1N 6N5

### ARTICLE INFO

#### Article history:

Received 27 June 2008

Accepted 22 December 2008

Available online 8 January 2009

#### Keywords:

Terrestrial cosmogenic nuclides

Supraglacial debris

Rockfalls

Erosion

Karakoram

Glaciers

### ABSTRACT

Basin-wide rockwall retreat rates are estimated using cosmogenic  $^{10}\text{Be}$  concentrations in supraglacial debris from the Baltoro Glacier basin in K2 region of the Central Karakoram, Pakistan. Total cosmogenic  $^{10}\text{Be}$  concentrations of the supraglacial debris were measured using accelerator mass spectrometry to determine  $^{10}\text{Be}$  concentrations inherited from the rockwalls within the glaciated basin. Given that rockfall induced by periglacial weathering and snow and ice avalanches is the most important source of supraglacial debris production in the high mountain glaciated basin, the erosion rate of the bare bedrock can be considered to be the rate of rockwall retreat. The rate of the rockwall erosion, converted from the calculated inheritance of  $^{10}\text{Be}$  concentrations, using the maximum velocity of the active glacier, places an upper limit ranging from 0.65 mm/year to 2.48 mm/year. This rate of rockwall retreat is in the same order of magnitude reported in other high Himalayan mountains. The rate, however, is an order of magnitude higher than erosion rates inferred from sediment budget studies and half that of the fluvial incision rate and exhumation rate for the same region. The difference between rates of basin-wide rockwall retreat and fluvial incision rates over the Late Quaternary suggests that in this glaciated basin fluvial incision is likely enhanced by localized/differential tectonism and/or isostatic uplift.

© 2008 Elsevier B.V. All rights reserved.

### 1. Introduction

Bedrock erosion is a key process in establishing the patterns of mountain geodynamics and landscape evolution within a specific basin. There is considerable controversy regarding the relative importance of surface processes and rates of erosion in high-mountain environments. This is especially true for glacial erosion, since it plays a role in isostatic and tectonic uplift, thereby influencing relief production, as well as erosion from periglacial processes (Shroder, 1993; Bishop et al., 2002, 2003; Shroder and Bishop, 2004). Unfortunately, estimating the magnitude of alpine glacier erosion is notoriously difficult, as is estimating the range and magnitude of erosion on steep slopes at high altitude (Whalley, 1984).

Until the advent of terrestrial cosmogenic nuclide (TCN) based erosion rates, two different methods have been used to define the rate of rockwall retreat by periglacial processes. The first is measuring the

volume of accumulated sediment in natural traps (Rapp, 1960; Andre, 1997; Matsuoka and Sakai, 1999) and/or artificial traps (Douglas, 1980) that had been derived from the headwalls of cirques. Rockwall retreat rates are then quantified by dividing the volume of stored sediment by catchment areas. In the second method, catchment-wide erosion rates have also been quantified by measuring the debris volume within rock glaciers of known ages (Humlum, 2000). More recently TCN methods allow rates of basin-wide erosion to be determined on geomorphic timescales ( $\leq 10^6$  years) for various climatic environments (Brown et al., 1995; Granger et al., 1996; Clapp et al., 2000; 2001; Bierman and Caffee, 2001; Schaller et al., 2001; Matmon et al., 2003; Vance et al., 2003; Seong et al., 2009a). Heimsath and McGlynn (2008) and Seong et al. (2009a) have applied this method to estimate rates of erosion for glacial catchments. Here we use this newly developed method to examine and define rates of basin-wide rockwall retreat for the world's highest topography, the K2 region of the Central Karakoram in Pakistan (Fig. 1).

Large valley glaciers in the western Himalaya are commonly characterized by extensive mass-movement-generated rock falls, and slides, debris falls and slides, and a variety of ice- and snow-avalanche deposition of rock materials. Many glaciers in the Himalaya are

\* Corresponding author. Present address: Department of Geography Education, Korea University, Seoul, 136-701, South Korea. Tel.: +82 10 7689 6160.

E-mail address: [ybseong@hotmail.com](mailto:ybseong@hotmail.com) (Y.B. Seong).

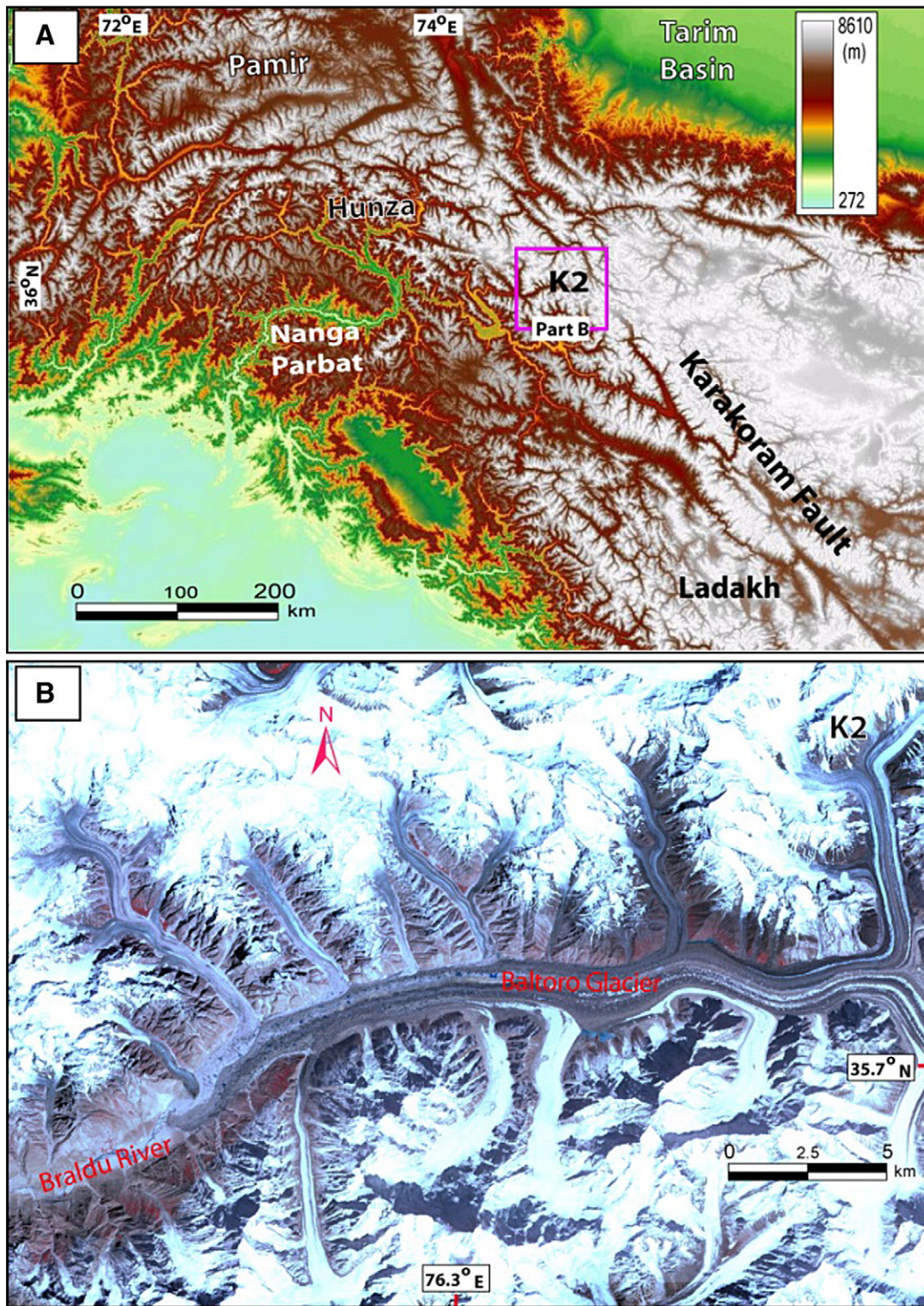


**Fig. 1.** Location of the study area (A) on a digital elevation model of the western end of Tibetan Himalayan orogen and (B) an ASTER image showing the Baltoro Glacier system. The Braldu River draining the study area flows from right to left.

classified either as incised-reservoir (*Firnessel*) types in deep, narrow valleys with multiple catchments that are fed largely by snow and ice avalanches, or avalanche (*Lawinen*) types that lack tributary reservoirs (Visser, 1938; Washburn, 1939). Such snow- and ice-avalanche processes mobilize huge amounts of debris that is first weakened and mobilized by strong freeze and thaw, or direct avalanche impact. Large talus and colluvial cones are observed to be debouching directly onto glacial ice in many places (Hewitt, 1993; Shroder, 1993; Shroder and Bishop, 2004). Thus at the base of steep mountain slopes lateral

moraine debris accumulates in huge amounts from the adjacent steep slopes, and where two glaciers join as tributaries, the resulting single medial moraine between them carries rock samples from both valleys.

The K2 region of the Central Karakoram is dominated by many glaciers >50 km in length (some of the world's longest outside of the polar and Alaskan regions), long bedrock slopes and extensive screes (Fig. 2; Seong et al., 2007; 2009b). The glaciers have extensive supraglacial debris cover, most of which is supplied to the glacier surface by mechanical weathering of the adjacent bedrock valley

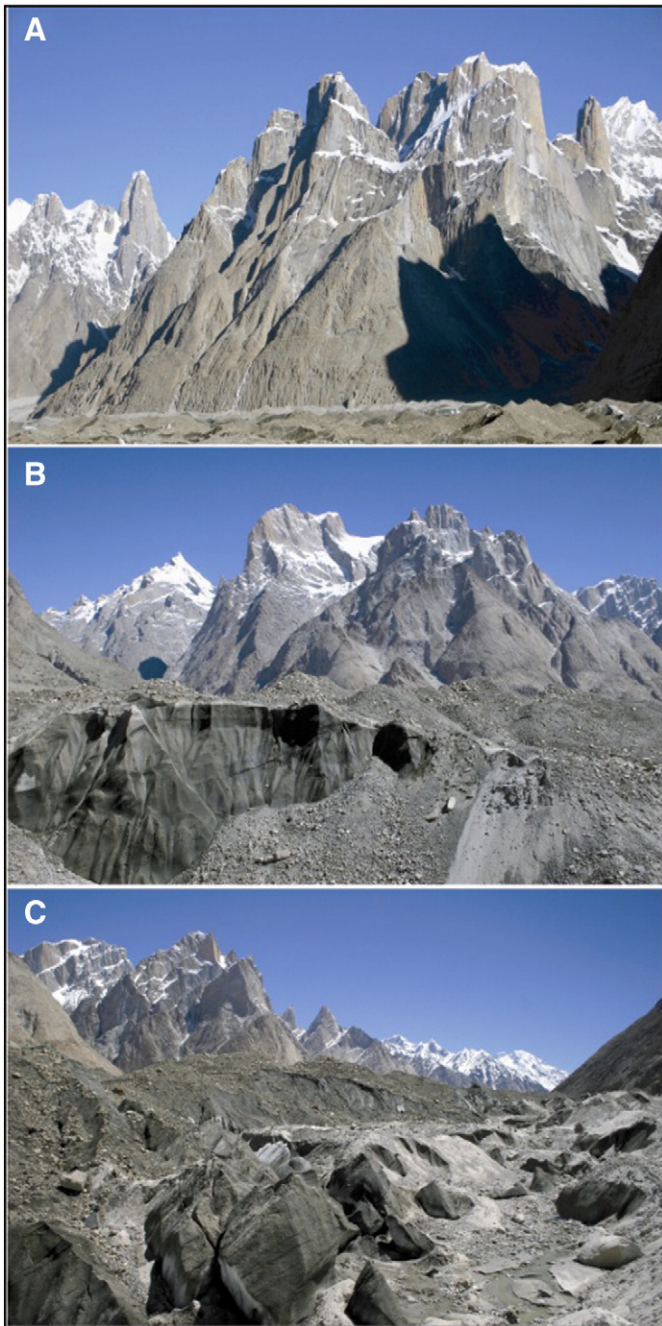


**Fig. 2.** Views of the Baltoro glacier system showing rockfall and supraglacial debris in the study area. (A) Rock faces of Trango Towers sourcing debris to the surface of the glacier (lowest part of frame). (B) Typical debris mantled surface (the debris is  $\leq 2$  m thick at this location). Note the truncating of the active glacier movements which could possibly elevate englacial and subglacial debris on the supraglacial debris system. Consequently, all the samples for cosmogenic  $^{10}\text{Be}$  analysis were collected above the any active truncating plane found. (C) Detailed review of supraglacial debris being modified by debris flow and glaciofluvial processes.

slopes due to diurnal and/or seasonal thermal changes that fracture the rock, and snow and ice avalanches and rockfalls that transport it to the glacier surface. This supraglacial debris is transported to the glacier snout to form impressive laterofrontal moraines, or is reworked by glaciofluvial and glacioeolian processes, and ultimately transported along and out of the main valleys. The steep topography is susceptible to gravitational detachment, and the supraglacial debris essentially reflects the amount of bedrock erosion in this region, and its TCN inventory reflects the magnitude of high-altitude basin-wide erosion.

In high mountain environments, such as the Karakoram, that have little vegetation and are frozen most of the year, rockfalls are one of the major geomorphic processes acting on the steep slope and thus retreating headwall (Whalley, 1984). There are several weathering processes contributing to generation of rockfall in steep, cold environments, in particular gelifraction and salt crystal weathering. Irrespective of any specific processes generating rockfall, most of the debris produced by rockfall should fall on to the glacier within a particular glaciated basin. The supraglacial debris is transported by the glacier acting like a conveyor belt and, ultimately evacuated into the proglacial system. Throughout the Himalaya, the ablation area of the glaciers mantled by thick debris is extensive (Benn and Lehmkuhl, 2000; Owen et al., 2003) and is likely to be mostly contributed by rockfalls and avalanches from the steep slopes of the headwall basin and surrounding valley-wall slopes. Quantifying rates of erosion and weathering, in various geomorphic and climatic settings and across different spatio-temporal scales, is central to understanding the styles and rates of landscape evolution. At present, the analysis of *in situ* produced TCNs is the only reliable way to quantify long-term (geomorphic) average ( $>10^3$ – $10^4$  years) erosion rates of bare bedrock surfaces (Lal, 1991; Gosse and Phillips, 2001). We define the headwall retreat rate of the glaciated basin supplying all of the debris to the K2 glacier system through rockfall activity using the inherited abundances of TCN  $^{10}\text{Be}$  of the supraglacial debris.

## 2. Study area

The study area is located in the Central Karakoram, which is situated at the western end of the Transhimalaya (Fig. 1). The Baltoro Glacier dominates the region and has a total length of  $\sim 58$  km. The Godwin Austen tributary Glacier advances from K2 (8611 m asl) to join the main Baltoro Glacier coming from the south, where they join at Concordia to flow west. The Baltoro Glacier is fed by many smaller glaciers, including the Uli Biaho Glacier, Trango, Liligo, and numerous other glaciers (Fig. 3). The valley trough occupied by the Baltoro and its tributaries can be very wide, reaching  $\sim 3$  km at Concordia, where the Godwin Austen and Upper Baltoro meet to form the main Lower Baltoro Glacier. Small valley glaciers form icefalls in some places where they meet the trunk glacier. The slope of sidewalls varies from very steep ( $>40^\circ$ ) to vertical. The glaciers have oscillated considerably during the Late Quaternary, extending more than 100 km beyond the present positions during the Late Pleistocene (Seong et al., 2007). The Baltoro Glacier provides the headwaters for the Braldu River that joins the Shigar River, which in turn is a tributary of the Indus River.

Snow accumulation on the glaciers of the Central Karakoram occurs mainly during the winter due to the penetration of mid-latitude westerlies, although significant late summer snowfall events can also occur at high altitudes due to the influence of the Indian Monsoon. Annual snow accumulation on the Biafo Glacier, adjacent to the study area, ranges from 0.9 to 1.9 m water equivalent, with maximum accumulation rates above altitudes of 4900 to 5400 m asl (Wake, 1989). Most current glaciers are of high-activity type, with high-altitude accumulation zones and relatively low ( $<10^\circ$ ) slopes (particularly in the ablation areas) compared to the surrounding topography (Andrews, 1975). The glaciers are fed by direct snowfall and extensive snow avalanching from steep slopes. The perennial ice and climate zone at high altitude comprises the very highest ridges and peaks including K2 (8611 m asl), Gasherbrum 1 (8068 m asl), Broad Peak (8047 m asl) and Gasherbrum II (8035 m asl) in the study area (Fig. 3). For many glaciers in the region, the ablation and accumulation zones areas are separated by steep icefalls or avalanche tracks. In the ablation zone of the Baltoro Glacier, the terminus regions are covered with extensive debris cover, which can be  $>4$  m or more in thickness (Seong et al., 2009b).

The Baltoro Glacier has more than 10 separated medial moraines above Concordia. Below Concordia all are squeezed together and form the main surface of the glacier (Figs. 1B and 3B). A number of additional smaller tributary glaciers below Concordia also add ice and rock mass to the main

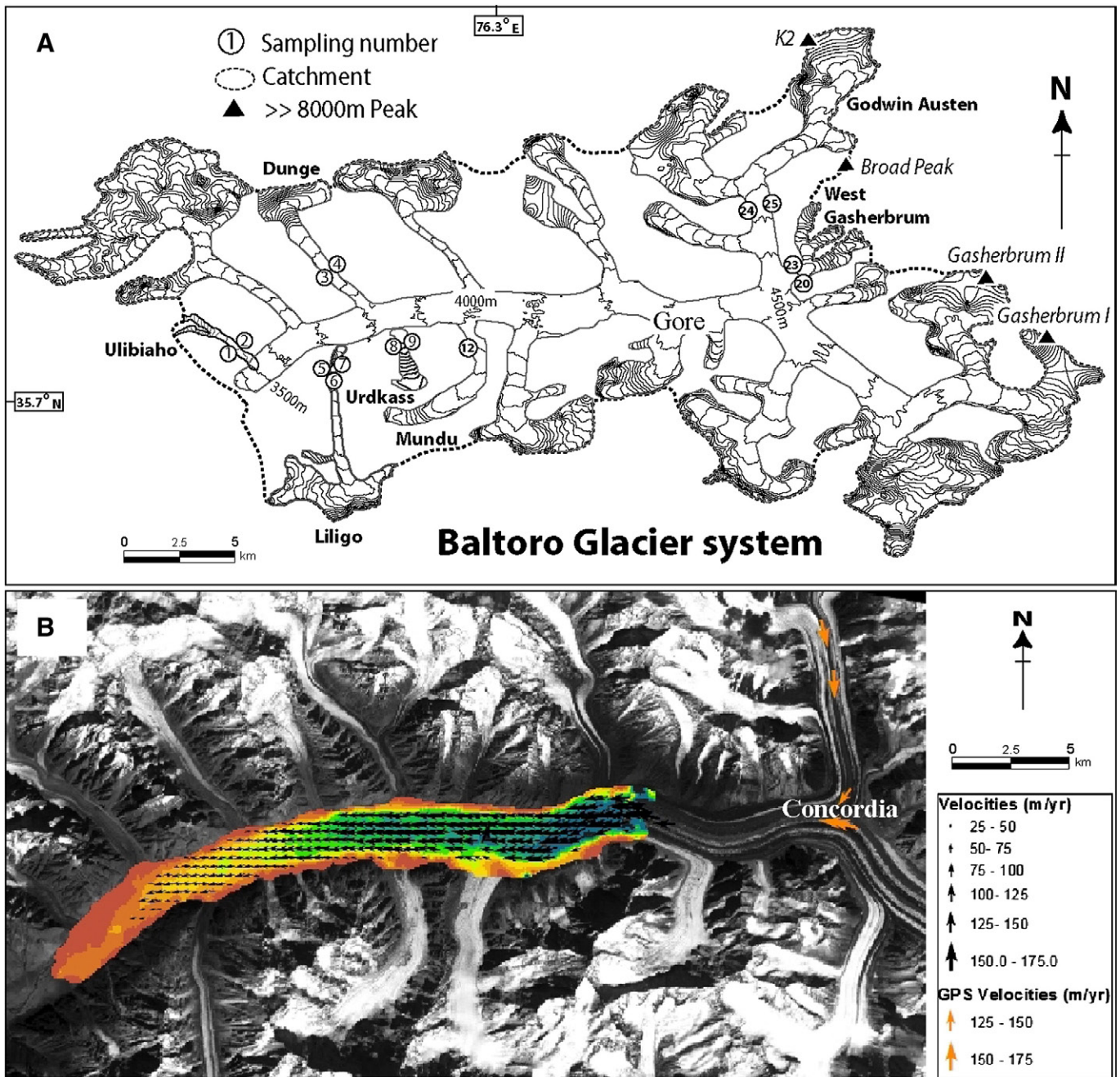


**Fig. 3.** (A) Locations of cosmogenic samples on the Baltoro Glacier system. Contour interval is 100 m. The 8000 m peaks in the study area include K2 (8611 m asl), Broad Peak (8047 m asl), Gasherbrum II (8035 m asl), and Gasherbrum I (8068 m asl). (B) Glacier velocity achieved by ASTER feature tracking along the Baltoro Glacier (Copland et al., in press).

ice stream. In the upper reaches above Concordia, where clean white ice streams dominate the icescape, the physical definition between medial moraines is most clear. Further down the main Baltoro Glacier below Concordia, the precise definition between separate medial moraines is lost as they blend together. Only where an especially distinctive rock type, such as for example, the light-colored granite of Uli Biaho and Trango glaciers brings it into juxtaposition next to such lithologies as the dominantly dark metasediments of the main Baltoro Glacier, can distinct boundaries be drawn. For this study we mapped medial moraines above Concordia, as well as collecting several distinct lithologies in one sample from the Baltoro drainage basin, in order to better characterize the supraglacial transport of this dominantly mass-movement-derived material.

The medial moraines of Concordia are quite distinct because most are separated by the previously noted white ice streams of the different glaciers that produced them, and because the moraines sample quite

diverse lithologies, ranging from low-grade metasedimentary rocks to various igneous rocks, and high-grade gneisses (Searle, 1991). The diverse lithologies are most commonly strongly color differentiated, with such things as “black” slates, “buff” metaclastics, and “gray” K2 gneisses, which makes them quite distinctive in appearance.

An important surficial aspect of the medial moraines above Concordia is their widths prior to major compression to less than half their original dimension through the Concordia chokepoint mouth and out into the main glacier valley. To study this aspect we measured the lengths and widths of white ice streams, together with that of the medial moraines, in order to gain a better understanding of flow dynamics and the change characteristic with distance traveled. In general, the distinctiveness of the different medial moraine lithology groupings is lost a few km down-ice from Concordia as the rock fragments are mixed progressively and blended together as more heterogeneous masses.

This extensive and thick supraglacial debris effectively insulates the glaciers at lower altitudes and reduces the rate of ablation (Shroder et al., 2000). At higher altitudes (4000–5500 m asl), thin layers of debris enhance ablation and result in the production of significant quantities of meltwater that eventually accumulate to form suprafluvial streams. In Himalayan environments, thick debris cover generally reduces sediment transfer by the glacier as the glacier activity and velocity is reduced, and ultimately can result in the formation of a rock glacier (Owen and England, 1998). Such availability of meltwater at higher altitudes is partly responsible for the high summer ice velocities, such as those we recorded in 2005 (Copland et al., in press).

### 3. Methods

Fieldwork was undertaken in the valleys from the snout of the Baltoro Glacier to the base of K2 during the summer of 2005. Geomorphologic mapping was conducted in the field and GPS measurements and ground photography were used as reference data to facilitate mapping from satellite imagery (including Landsat ETM+ data acquired on October 17, 1999 and ASTER multispectral imagery data acquired on August 12, 2000). In addition, topographic maps (1:50,000; 1:25,000) of the region supplied by the Government of Pakistan were used to aid in the identification of landforms. All multispectral satellite data were orthorectified to account for relief distortion. Topographic characteristics for each basin of the glacier system were analyzed using a digital elevation model (DEM), which was constructed from ASTER stereo 3N and 3B images. During the same field campaign, Copland et al. (in press) determined ice depths using GPR (Ground Penetrating Radar) and surface ice velocities with repeat differential GPS measurements at fixed markers. The point GPS measurements were then used to verify velocities calculated across the entire ablation area of the Baltoro Glacier from feature tracking using pairs of clear-sky multitemporal ASTER satellite scenes (Scambos et al., 1992). The basin-wide average velocities were used to calculate TCN  $^{10}\text{Be}$  concentrations in the supraglacial sediments on the glacier during transportation.

We collected a total of 25 aggregate samples from the supraglacial debris on the active ice on the Baltoro Glacier (Table 1). Most samples were taken from distinct lateral moraines and the other samples (K2E-6, K2E-20, K2E-23, K2E-24, and K2E-25) were collected from the hummocky glacier surface, which did not form distinct moraines. In the field, aggregate samples were sieved using a 1000  $\mu\text{m}$  diameter

**Table 1**  
Sampling locations for supraglacial debris on the Baltoro Glacier system and  $^{10}\text{Be}$  TCN concentrations measured.

	Latitude (°N)	Longitude (°E)	Altitude (m)	Quartz (g)	Production rate (atoms/g-year) <sup>a</sup>	$^{10}\text{Be}$ ( $10^4$ atoms/g)
K2E-1	35.704	76.161	4484	15.1	84.02	5.78 ± 0.34
K2E-2	35.708	76.166	4483	15.4	83.98	4.68 ± 0.31
K2E-3	35.744	76.236	5216	16.1	117.87	4.61 ± 0.60
K2E-4	35.749	76.243	5218	15.3	117.97	5.87 ± 0.32
K2E-5	35.703	76.221	5075	15.1	110.70	4.67 ± 0.43
K2E-6	35.703	76.223	5091	15.3	111.50	4.42 ± 0.27
K2E-7	35.700	76.225	5127	15.2	113.31	9.97 ± 0.44
K2E-8	35.723	76.252	4659	15.1	91.37	5.23 ± 0.35
K2E-9	35.722	76.258	4641	15.1	90.60	5.32 ± 0.33
K2E-12	35.733	76.316	4103	15.2	125.14	6.75 ± 0.44
K2E-20	35.765	76.535	4655	6.6	157.51	11.68 ± 2.19
K2E-23	35.758	76.536	4643	15.1	160.72	4.22 ± 0.36
K2E-24	35.821	76.513	4869	14.4	170.64	15.54 ± 0.75
K2E-25	35.822	76.516	4877	15.0	170.30	6.04 ± 0.61

<sup>a</sup> Production rates were calculated using Stone (2000) scaling factors; sea-level high-latitude (SLHL) production rate = 4.98  $^{10}\text{Be}$  atoms/g quartz per year; zero erosion rate; asl—above sea level. Uncertainties include analytic errors (weighing of sample, weighing and concentration of spike, and AMS error) and attenuation length. Uncertainties related to production rate and scaling factors were not explicitly treated here. The altitudes for calculation of  $^{10}\text{Be}$  production rate in the supraglacial debris were averaged considering area–altitude distribution from the sampling locations to upglacier.

mesh. All the samples were collected upglacier beyond any glacial thrust blocks to avoid the contribution of any englacial and subglacial debris to the samples. The latitude, longitude, elevation, and aspect were recorded for each of the samples (Table 1).

All samples were prepared in the geochronology laboratories at the University of Cincinnati. Amalgamated samples were dried in the oven and sieved again into the 250–500  $\mu\text{m}$  size fraction. Quartz was then separated using the method of Kohl and Nishiizumi (1992). After addition of low background  $^9\text{Be}$  carrier ( $^{10}\text{Be}/^9\text{Be} = 1 \times 10^{-15}$ ), Be was separated and purified by ion exchange chromatography and precipitated at  $\text{pH} > 7$ . The hydroxides were oxidized by ignition in quartz crucibles. BeO was mixed with Nb metal and loaded onto targets for the determination of the  $^{10}\text{Be}/^9\text{Be}$  ratio by accelerator mass spectrometry at the Prime Laboratory of Purdue University. Isotope ratios were compared to ICN Pharmaceutical, Incorporated  $^{10}\text{Be}$  standards prepared by K. Nishiizumi (Nishiizumi et al., 2007) and using a  $^{10}\text{Be}$  half-life of  $1.36 \times 10^6$  year. The measured isotope ratios were converted to TCN concentrations in quartz using the total  $^{10}\text{Be}$  in the samples and the sample weights. TCN  $^{10}\text{Be}$  concentrations were then converted to steady-state erosion rate using a sea level high latitude (SLHL)  $^{10}\text{Be}$  production rate of 4.98 atom per gram of quartz per year (Lal, 1991; Stone, 2000; Balco et al., 2008). Scaling factors were applied to compensate for altitude-dependent effect in calculating cosmic ray exposure ages (Stone, 1999). The error range for the converted erosion rate is shown as one standard deviation (e.g.  $10 \text{ m Ma}^{-1} \pm 1\sigma$ ).

To calculate the  $^{10}\text{Be}$  concentrations of the supraglacial debris, we used the equation of Lal (1991) for an eroding surface, where:

$$N(t) = \frac{P(0)}{\lambda + \mu\varepsilon} (1 - e^{-(\lambda + \mu\varepsilon)t}), \quad (1)$$

such that  $N(t)$  is the surface concentration at steady-state exposure time ( $t$ ) (atoms  $^{10}\text{Be}$   $\text{g}^{-1}$  quartz),  $P(0)$  is the production rate at the surface (atoms  $^{10}\text{Be}$   $\text{g}^{-1}$  quartz),  $\lambda$  is decay constant for  $^{10}\text{Be}$ ,  $\mu$  is the absorption coefficient ( $160 \text{ cm}^{-1}$ ), and  $\varepsilon$  is the surface erosion (Lal, 1991). The average production rate on a glacier catchment was calculated using the area–altitude distribution of the catchment and topographic shielding at the mid-point of the catchment (Fig. 4; Table 2). The concentration of *in situ* produced TCNs in eroding surfaces can be modeled for determining steady-state erosion rate of the bedrock surface as well as surface exposure age (Lal, 1991; Small et al., 1997). A TCN becomes saturated (secular equilibrium) after prolonged steady-state erosion when  $t \gg 1/(\lambda + \mu\varepsilon)$ . That is, steady-state erosion must have removed a layer of rock equivalent to two or more erosion cosmic-ray attenuation depths ( $1/\mu$ ). Erosion is steady-state if constant on the time scale of TCN accumulation. Under these circumstances, a measured concentration can be interpreted in terms of a maximum, steady-state erosion rate (Lal, 1991).

To determine basin-averaged erosion rates of the headwall area contributing all the supraglacial debris by rockfall on to the glacier system, inherited TCN concentrations were obtained by subtracting the abundances produced during transportation from the inventories of  $^{10}\text{Be}$  measured for selected supraglacial debris (Table 2). The inheritance that was likely to accumulate in the rockwall surface can be converted into the steady-state erosion rate applying the following equation (Lal, 1991; Table 3):

$$\varepsilon = \frac{\Lambda}{\rho} \left( \frac{P(0)}{N_i} - \lambda \right) \quad (2)$$

Where,  $N_i$  is inherited activity (atoms  $^{10}\text{Be}$   $\text{g}^{-1}$  quartz),  $P(0)$  is the production rate at the surface,  $\varepsilon$  is erosion rate ( $\text{cm year}^{-1}$ ),  $\rho$  is density of the target material ( $\text{g cm}^{-3}$ ), and  $\Lambda$  is attenuation depth ( $150 \text{ g cm}^{-2}$ ). Accordingly, the calculated erosion rate may be equal to the rate of rockwall retreat, assuming all the debris has fallen by rockfall and avalanche from the walls of the basin.

Centerline ice flow velocities on the Baltoro Glacier were measured in the summer of 2005 at between 10 m/year at the glacier terminus

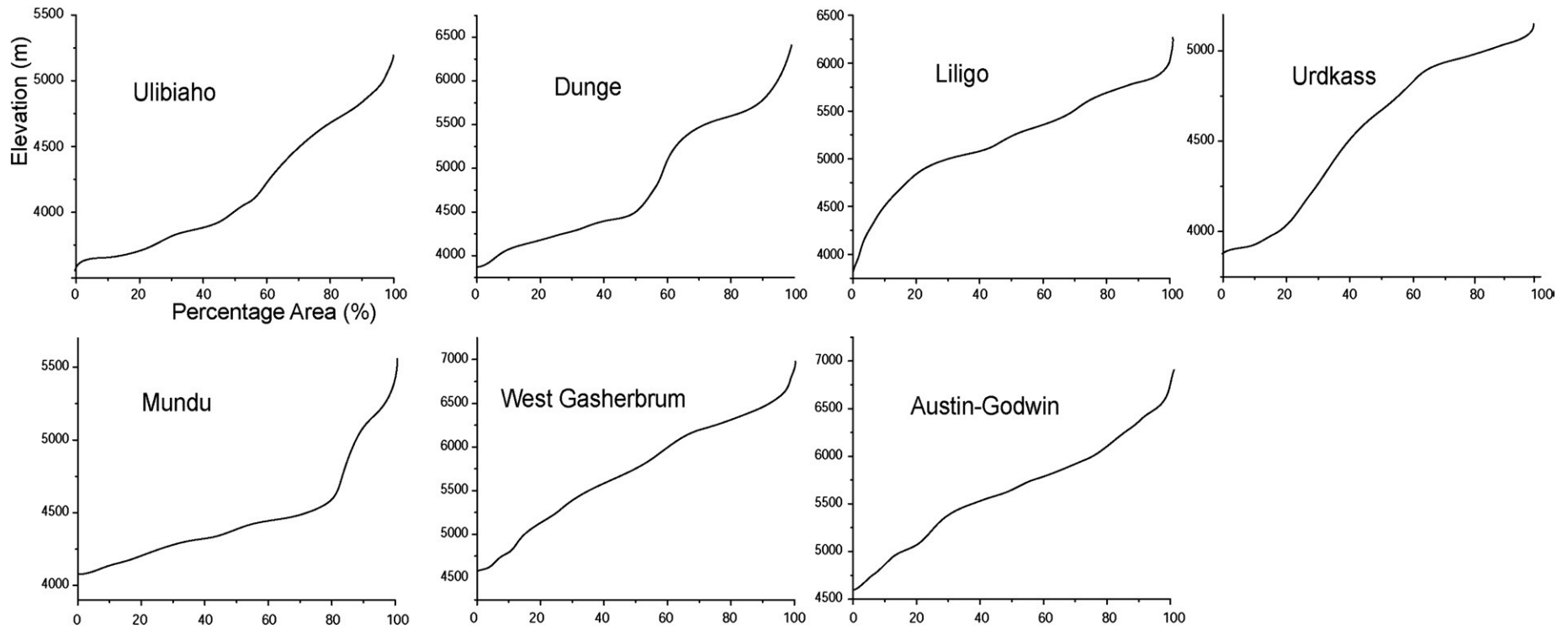


Fig. 4. Area–altitude distribution of the basins used to calculate the basin-wide <sup>10</sup>Be cosmogenic nuclide production rate for each sample.

**Table 2**Travel distance and duration, production rate in the supraglacial debris on the conveyor belt system during glacier transportation, and inventories of inherited  $^{10}\text{Be}$  TCNs.

	Location	Annual average velocity of glacier (m/year) <sup>c</sup>	Longest distance of debris transportation (m) <sup>d</sup>	Travel time (year) <sup>e</sup>	$^{10}\text{Be}$ (10 <sup>4</sup> atoms/g)	Mean elevation <sup>f</sup>	Mean production rate during transportation (atoms/g-year) <sup>g</sup>	Max. $^{10}\text{Be}$ production during transportation (10 <sup>4</sup> atoms/g) <sup>h</sup>	Min. $^{10}\text{Be}$ production during transportation (10 <sup>3</sup> atoms/g) <sup>i</sup>	Max. inherited $^{10}\text{Be}$ (10 <sup>4</sup> atoms/g) <sup>j</sup>	Min. inherited $^{10}\text{Be}$ (10 <sup>3</sup> atoms/g) <sup>k</sup>
K2E-1	LM <sup>a</sup>	25–175	4850	28–471	5.78 ± 0.34	3875	61.77	1.20	1.71	5.61 ± 0.34	4.59 ± 0.27
K2E-2	LM	25–175	4840	28–470	4.68 ± 0.31	3875	61.77	1.20	1.71	4.51 ± 0.31	3.49 ± 0.24
K2E-3	LM	25–175	9620	55–934	4.61 ± 0.60	4274	75.78	2.92	4.17	4.20 ± 0.60	1.70 ± 0.24
K2E-4	LM	25–175	9690	55–941	5.87 ± 0.32	4274	75.78	2.94	4.20	5.45 ± 0.32	2.93 ± 0.17
K2E-5	LM	25–175	13,230	76–1284	4.67 ± 0.43	4681	92.33	4.89	6.98	3.98 ± 0.43	N.A. <sup>l</sup>
K2E-6	SD <sup>b</sup>	25–175	13,150	75–1277	4.42 ± 0.27	4681	92.33	4.86	6.94	3.73 ± 0.27	N.A.
K2E-7	LM	25–175	13,090	75–1271	9.97 ± 0.44	4681	92.33	4.83	6.91	9.28 ± 0.44	5.13 ± 0.24
K2E-8	LM	25–175	3140	18–305	5.23 ± 0.35	4286	76.23	0.96	1.37	5.10 ± 0.35	4.28 ± 0.29
K2E-9	LM	25–175	3210	18–312	5.32 ± 0.33	4286	76.23	0.98	1.40	5.18 ± 0.33	4.34 ± 0.28
K2E-12	LM	25–175	10,200	58–990	6.75 ± 0.44	4363	79.20	3.23	4.62	6.29 ± 0.44	3.52 ± 0.24
K2E-20	SD	25–175	7890	45–766	11.68 ± 2.19	5422	128.92	4.07	5.81	11.10 ± 2.19	7.62 ± 0.15
K2E-23	SD	25–175	7280	42–707	4.22 ± 0.36	5422	128.92	3.75	5.36	3.68 ± 0.36	0.46 ± 0.04
K2E-24	SD	25–175	14,780	84–1435	15.54 ± 0.75	5530	135.00	7.98	11.40	14.40 ± 0.75	7.56 ± 0.39
K2E-25	SD	25–175	14,920	85–1449	6.04 ± 0.61	5530	135.00	8.06	11.81	4.89 ± 0.21	N.A.

<sup>a</sup> LM indicates lateral moraine.<sup>b</sup> SD indicates supraglacial debris which was not inset into the moraines.<sup>c</sup> Measured from differential GPS measurement and ASTER feature tracking by Copland et al. (in press).<sup>d</sup> Longest distances during transportation of supraglacial debris from the most distant point upglacier to the sampling location on each glacier basin.<sup>e</sup> Duration the glacier takes to transport the supraglacial debris along the longest distance at a rate of transportation measured in Copland et al. (in press).<sup>f</sup> Average elevation corrected for the distribution pattern of area–altitude in the glacier basin.<sup>g</sup> Average production rate of cosmogenic  $^{10}\text{Be}$  in the quartz embedded in the supraglacial debris during transportation along the longest pathway.<sup>h</sup> Total cosmogenic  $^{10}\text{Be}$  production during transportation of supraglacial debris along the longest pathway at a slowest rate of 25 m/year.<sup>i</sup> Total cosmogenic  $^{10}\text{Be}$  production during transportation of supraglacial debris along the longest pathway at a fastest rate.<sup>j</sup> Maximum inherited  $^{10}\text{Be}$  were calculated by the deduction of  $^{10}\text{Be}$  produced during transportation from the concentration measured.<sup>k</sup> Minimum inherited  $^{10}\text{Be}$  were inferred by the deduction of  $^{10}\text{Be}$  produced during transportation from the concentration measured.<sup>l</sup> N.A. not available because the value is less than zero.

(3500 m asl) and a maximum of 245 m/year at the altitude of 4300 m asl. At altitudes higher than Gore, which is somewhat below the equilibrium line altitude (ELA) of the Baltoro Glacier system and thus basal sliding velocity reduces due to lower melt water availability in the bed upvalley, velocities gradually decreased to 160 m/year at K2 base camp (4850 m). For this study, we used the slowest and fastest values measured in the field, respectively. However, given that most of the supraglacial debris collected for TCN  $^{10}\text{Be}$  analysis came from the upper reaches of the glacier, the minimum measured velocity of the glacier is likely to be less reasonable. In particular, the overall velocity

of the glacier became slower toward the terminus of the glacier. Thus, we assume the maximum value of the glacier velocity obtained by ASTER feature tracking might be a more realistic number, but this might not be appropriate over long time frames (>10<sup>2</sup> years). Using minimum and maximum values, however, takes into account possible uncertainty and provides the best estimate for the likely erosion rates.

To obtain the inherited concentration of TCN  $^{10}\text{Be}$  of the supraglacial debris before it was incorporated into the active supraglacial debris transportation system, a series of separate computations were carried out (Table 2). Transported distances from the sourcing surface to the locations where supraglacial debris were sampled were calculated using a digital elevation model generated from ASTER scenes. The longest pathways range in horizontal distance from 3140 to 14,920 m depending on the length of the glacier. The transporting distances were converted into travel time following the longest pathways, ranging from 18 to 1435 years considering the centerline velocity of the glaciers estimated by feature tracking. The TCN  $^{10}\text{Be}$  abundances produced during the transportation by the glacier acting like a conveyor belt are calculated using TCN  $^{10}\text{Be}$  production rate corrected for area–altitude distribution. Ultimately, the inherited concentrations of the supraglacial debris were used to estimate the erosion rate of the rockwall from which all the debris was delivered onto the glacier. Given all the debris produced from the rockwall of the glacier basin by rockfalls and avalanches (excluding any eolian contribution), the erosion rate of rockwall can be regarded as the average rate of rockwall retreat in the glaciated basin.

#### 4. Results

Although quantifying the erosion rate of the headwall of active glacier is challenging, measured abundances of TCN  $^{10}\text{Be}$  from supraglacial debris allowed us to infer the retreat rate of the rockwalls by periglacial weathering and mass-movement processes ranges from 0.65 mm/year to 2.48 mm/year (1.27 ± 0.53 mm/year; Table 3). This apparent rate of basin-wide erosion is likely, however, to be the upper limit of long-term erosion rate because we used maximum velocity of

**Table 3**

Inferred basin-wide rockwall retreat rate.

Glacier	Basin mean altitude (m) <sup>a</sup>	Production rate (atoms/a) <sup>b</sup>	Max. erosion rate of Rockwall (mm/year)	Min. erosion rate of Rockwall (mm/year)	
K2E-1	Ulibiaho	4621	89.74	0.97 ± 0.06	0.01 ± 0.00
K2E-2	Ulibiaho	4621	89.74	1.20 ± 0.08	0.02 ± 0.00
K2E-3	Dunge	4742	95.02	1.37 ± 0.20	0.03 ± 0.00
K2E-4	Dunge	4742	95.02	1.05 ± 0.06	0.02 ± 0.00
K2E-5	Liligo	5406	128.04	1.95 ± 0.21	N.A. <sup>c</sup>
K2E-6	Liligo	5406	128.04	2.08 ± 0.21	N.A.
K2E-7	Liligo	5406	128.04	0.83 ± 0.04	0.02 ± 0.00
K2E-8	Urdkass	4507	84.96	1.01 ± 0.07	0.01 ± 0.00
K2E-9	Urdkass	4507	84.96	0.99 ± 0.06	0.01 ± 0.00
K2E-12	Mundu	4883	101.45	0.97 ± 0.07	0.02 ± 0.00
K2E-20	West	5797	150.91	0.82 ± 0.16	0.01 ± 0.00
K2E-23	West	5797	150.91	2.48 ± 0.24	0.20 ± 0.02
K2E-24	Godwin Austen	5877	155.92	0.65 ± 0.03	0.01 ± 0.00
K2E-25	Godwin Austen	5877	155.92	1.93 ± 0.24	N.A.

<sup>a</sup> Average altitude of the basin as a sourcing area considered only rockwall area (excluding active glacier area).<sup>b</sup> Basin-wide average production rate of  $^{10}\text{Be}$  were determined considering area–altitude distribution of only rockwall basin.<sup>c</sup> N.A. means not available.

the glacier to infer the inherited concentration of TCN  $^{10}\text{Be}$  from supraglacial debris transported by the glacier acting like a conveyor belt. Two groups of samples were collected for evaluating the degree of mix-up of the supraglacial sediments. Most of the samples were taken from lateral moraines and five samples (K2E-6, K2E-20, K2E-23 through K2E-25) were collected from the supraglacial debris existing between the lateral moraines. Although all the inferred erosion rates are somewhat variable, they are centered between 1 mm/year and 2 mm/year. Thus, our data show the measurement of the inherited concentration of TCN  $^{10}\text{Be}$  from the supraglacial debris works well for inferring the rate of rockwall retreating by periglacial weathering and mass-movement erosion in the headwalls of the active glaciers.

## 5. Discussion

Rock debris falling from the precipitous sidewalls of the cirques or valley walls is one of the most important processes for debris delivery to the active glacier systems (Boulton and Eyles, 1979; Ballantyne and Harris, 1994). Rockfall occurring in ice-free sidewalls of the glaciated basin are mainly associated with periglacial weathering resulting from annual and diurnal temperature cycles, coupled with erosion by the ubiquitous avalanches. Rockfall activity is mainly controlled by rock slope form, aspect, lithology, and geological structure (Benn and Evans, 1996).

Climate variations also play an important role in regulating snow accumulation and avalanching, as precipitation from the westerlies and the southwestern monsoon impacts erosion rates. In 2005, for example, this region received extreme amounts of snow by the westerlies, which caused an increase in the frequency of snow avalanches and debris flows due to increased melting and runoff at higher altitudes. We witnessed these occurrences in the field while working on the Baltoro Glacier. The region also receives summer snowfall from the monsoon that contributes to the magnitude of erosion. The climate dynamics of the region are complex, and climate station data, climate reanalysis data, and more direct assessments of precipitation within the region (TRMM data) suggests increases in precipitation. If this is the case, we might expect a greater frequency of mass movement process that could increase periglacial rates of erosion.

Previous studies that report present-day ( $\approx 1000$  years) rates of rockwall retreat indicate rates between 0.05 and 3.00 mm/year (Ballantyne and Harris, 1994). However, long-term ( $10^3$  to  $10^5$  years) rates of debris delivery onto the glacier surface by rockfalling are poorly known. In particular, the amount of debris onto the glacier surfaces by individual rockfall varies considerably in the magnitude of the debris, ranging from single particles to huge rock avalanches. Thus, long-term rates of rockwall retreat are essential in order to evaluate how fast glaciated basins erode via non-glacial processes.

Previous research focuses on the ice-free areas under periglacial environments because it is relatively easy to access. Conversely, there is a paucity of research on measuring the rate of headwall retreat that contributes to the supraglacial debris, with the exception of the pioneering work by Heimsath and McGlynn (2008). They inferred the rate of headwall retreat (0.01 to 2.15 mm/year) from supraglacial sediment flux measured over the summer. The supraglacial sediment flux is, however, likely to dramatically fluctuate as it responds to glacier meltwater variations, glacier flow velocity, basin geological conditions, and depends upon the magnitude and frequency of mass movements occurring on variable topography. In fact, the magnitude of these periglacial processes are all interpreted to the complex feedback mechanism of climate forcing, glacier erosion and uplift, which regulates glacier processes and the geomorphometry of the topography. Numerous feedbacks dictate the magnitude and spatio-temporal variability of non-glacial rates of erosion (Andre, 1997). Consequently, it is essential to better characterize these complexities and obtain more estimates of long-term rates of rockwall retreat.

Our average rate of rockwall retreating ( $1.27 \pm 0.53$  mm/year) is in the same range as that (0.01 to 2.15 mm/year) measured in Nepal

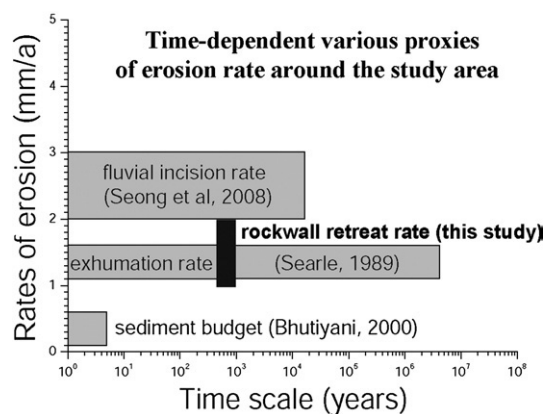


**Fig. 5.** Comparison of inferred periglacial weathering rate with other proxy records of erosion rate studied in the Central Karakoram (Searle et al., 1989; Bhutiayani, 2000; Seong et al., 2008).

Himalaya based on short-term supraglacial flux (Heimsath and McGlynn, 2008). This rate, however, contrasts with the glacial erosion rates (0.11 to 0.46 mm/year) measured by 5 years' sediment budget study for the Siachen glacier in the Nubra Valley, which is  $\sim 50$  km away located to the south (Bhutiayani, 2000; Fig. 5). The discrepancy in adjacent two regions may reflect different rates of evacuation of sediments by glacier and proglacial systems. Alternatively it might reflect differences between catchment areas and glaciers. However the two glacier systems drain from the same massif and have similar geology. Moreover, erosion rates inferred from sediment budget study are likely to ignore dissolved load, and underestimate the overall erosion rates of the glaciated basin. Fluvial incision rates determined by Seong et al. (2008) for the Braldu River, which drains the Baltoro Glacier, are double that of the average headwall retreat rates (1.27 mm/year), ranging from 2 to 3 mm/year for the last 11 ka, in our study (Fig. 5).

In our study area, glaciation was very extensive over the last few glacial cycles and thus was likely to be a more erosive agent than the other surface processes (Seong et al., 2007), although the magnitude of glacier erosion could still be relatively high, because of the increased meltwater production due to increased temperatures at high-altitude, and thin debris-cover at altitude, that enhances ablation. This can cause an increase in ice flow velocities and basal water pressure that affects erosion. The maximum erosion rate by periglacial weathering and avalanches suggests that erosion by headwall retreat is not keeping pace with downstream fluvial incision rates during the Holocene. This may possibly result from isostatic rebound of the area since the Holocene, and or by relatively high glacial erosion rates causing an influx of mass. More work on estimating glacier erosion rates is sorely needed. Collectively, the landscape evolution of the K2 region of the Central Karakoram exhibits highly variable rates of erosion caused by fluvial, glacial, and periglacial processes. A better understanding these complex glacial systems is required to provide more insight into periglacial processes and the magnitude of headwall retreat rates.

## 6. Conclusion

We provide the first quantitative estimates for average rates of basin-wide rockwall retreat using TCN  $^{10}\text{Be}$  from the supraglacial debris of the Baltoro Glacier system in the K2 region of the Central Karakoram, Pakistan. Rates of erosion ranged from 0.65 mm/year to 2.48 mm/year, using minimum and maximum ice-flow velocities derived from differential GPS. We equate our mean rate of erosion to reflect the average rate of rock-wall retreat within glaciated basins, as periglacial weathering and mass movement are the dominant processes that ultimately generate supraglacial debris. The average rate of rockwall retreat is the same order of magnitude as that reported in other high

mountain environments. Our average rate, however, is an order of magnitudes greater than the rate inferred from sediment budget studies and half that of the fluvial incision rate for the same study area. This discrepancy suggests that even in highly glaciated basins denudation may not be keeping pace on geomorphic timescales ( $10^5$  years) with the rapid fluvial incision enhanced by tectonic/or isostatic uplift.

## Acknowledgements

We would especially like to acknowledge the long-term and highly fruitful relationship with the late Syed Hamidullah, former Director of the Centre of Excellence at Peshawar University, who worked so much to help facilitate this project. We would also like to thank his students, Faisal Khan and Mohammad Shahid, for their excellent assistance in the field. This research was supported by funding from the National Geographic Society and the US National Science Foundation (Grant BCS-0242339) to the University of Nebraska–Omaha and the University of Cincinnati. This research was partially supported by a Meyer's Fellowship at the University of Cincinnati and supported by the Korea Research Foundation Grant funded by the Korean Government (KRF-2008-314-C00394) during the writing and revision of the manuscript. Thanks to Arjen Heimsath for sharing his thoughts and providing us with a pre-print of his paper in periglacial erosion in the Nepal High Himalaya.

## References

- Andre, M.F., 1997. Holocene rockwall retreat in Svalbard: a triple-rat evolution. *Earth Surface Processes and Landforms* 22, 423–440.
- Andrews, J.T., 1975. *Glacial Systems: An Approach to Glaciers and Their Environments*. Wadsworth Publishers Co, Duxbury, London.
- Balco, G., Stone, J.O., Lifton, N.A., Dunai, T.J., 2008. A complete and easily accessible means of calculating surface exposure ages or erosion rates from  $^{10}\text{Be}$  and  $^{26}\text{Al}$  measurements. *Quaternary Geochronology* 3 (3), 174–195.
- Ballantyne, C.K., Harris, C., 1994. *The Periglaciation of Great Britain*. Cambridge University Press, Cambridge.
- Benn, D.I., Evans, D.J.A., 1996. *Glaciers and Glaciation*. Arnold, p. 219.
- Benn, D.I., Lehmkuhl, F., 2000. Mass balance and equilibrium-line altitudes of glaciers in high mountain environments. *Quaternary International* 65/66, 15–29.
- Bhutiyan, M.R., 2000. Sediment load characteristics of a proglacial stream of Siachen Glacier and the erosion rate in Nubra valley in the Karakoram Himalayas, India. *Journal of Hydrology* 227, 84–92.
- Bierman, P.R., Caffee, M., 2001. Steady state rates of rocks surface erosion and sediment production across the hyperarid Namib Desert and the Namibian escarpment, southern Africa. *American Journal of Science* 301, 326–358.
- Bishop, M.P., Shroder Jr., J.F., Bonk, R., Olsenholler, J., 2002. Geomorphic change in High-Mountains: a Western Himalayan perspective. *Global and Planetary Change* 32 (4), 311–329.
- Bishop, M.P., Shroder Jr., J.F., Colby, J.D., 2003. Remote sensing and geomorphometry for studying relief production in high mountains. *Geomorphology* 55, 345–361.
- Boulton, G.S., Eyles, N., 1979. Sedimentation by valley glaciers: a model and genetic classification. In: Schluchter, C. (Ed.), *Moraines and Varves*. Balkema, Rotterdam, pp. 11–23.
- Brown, E., Stallard, R.F., Larsen, M.C., Raisbeck, G.M., Yiu, F., 1995. Denudation rates determined from the accumulation of in situ-produced  $^{10}\text{Be}$  in the Luquillo Experimental Forest, Puerto Rico. *Earth and Planetary Science Letters* 129, 193–202.
- Clapp, E.M., Bierman, P.R., Schick, A.P., Lekach, J., Enzel, Y., Caffee, M., 2000. Sediment yield exceeds sediment production in arid region drainage basins. *Geology* 28, 995–998.
- Clapp, E.M., Bierman, P.R., Nichols, K.K., Pavich, M., Caffee, M., 2001. Rates of sediment supply to arroyos from upland erosion determined using in situ produced cosmogenic  $^{10}\text{Be}$  and  $^{26}\text{Al}$ . *Quaternary Research* 55, 235–245.
- Copland, L., Bishop, M.P., Bush, A., Clendon, P., Copland, P., Finkel, R., Kamp, U., Owen, L.A., Seong, Y.B., Shroder, J.F., in press. Glacier velocities across the Karakoram Himalaya. *Annals of Glaciology* 52A042.
- Douglas, G.R., 1980. Magnitude frequency study of rockfall in Co. Antrim, N. Ireland. *Earth Surface Processes and Landforms* 5, 123–129.
- Gosse, J.C., Phillips, F.M., 2001. Terrestrial in situ cosmogenic nuclides: theory and application. *Quaternary Science Reviews* 20, 1475–1560.
- Granger, D.E., Kirchner, J.W., Finkel, R., 1996. Spatially averaged long-term erosion rates measured from in-situ produced cosmogenic nuclide in alluvial sediments. *Journal of Geology* 104, 249–257.
- Heimsath, A.M., McGlynn, R., 2008. Quantifying periglacial erosion in the Nepal high Himalaya. *Geomorphology*, 97 (1–2), 5–23.
- Hewitt, K., 1993. Altitudinal organization of Karakoram geomorphic processes and depositional environments. In: Shroder Jr., J.F. (Ed.), *Himalaya to the Sea*. Routledge, London, pp. 159–183.
- Humlum, O., 2000. The geomorphic significance of rock glaciers: estimates of rock glacier debris volumes and headwall recession rates in West Greenland. *Geomorphology* 35, 41–67.
- Kohl, C.P., Nishiizumi, K., 1992. Chemical isolation of quartz for measurement of in-situ produced cosmogenic nuclides. *Geochimica et Cosmochimica Acta* 56, 3583–3587.
- Lal, D., 1991. Cosmic ray labeling of erosion surfaces: in situ nuclide production rates and erosion models. *Earth and Planetary Science Letters* 104, 429–439.
- Matmon, A., Bierman, P.R., Larsen, J., Southworth, S., Pavich, M., Caffee, M., 2003. Temporally and spatially uniform rates of erosion in the southern Appalachian Great Smoky Mountains. *Geology* 31 (2), 155–158.
- Matsuoka, N., Sakai, H., 1999. Rockfall activity from an alpine cliff during thawing periods. *Geomorphology* 28, 309–328.
- Nishiizumi, K., Imamura, M., Caffee, M.W., Southon, J.R., Finkel, R.C., McAninch, J., 2007. Absolute calibration of  $^{10}\text{Be}$  AMS standards. *Nuclear Instruments and Methods in Physics Research Section B* 258 (2), 403–413.
- Owen, L.A., England, J., 1998. Observations on rock glaciers in the Himalayas and Karakoram Mountains of northern Pakistan and India. *Geomorphology* 26, 199–213.
- Owen, L.A., Derbyshire, E., Scott, C.H., 2003. Contemporary sediment production and transfer in high-altitude glaciers. *Sedimentary Geology* 155, 13–36.
- Rapp, A., 1960. Recent development of mountain slopes in Karveagge and surroundings, Northern Scandinavia. *Geografiska Annaler* 42A, 65–200.
- Scambos, T.A., Dutkiewicz, M.J., Wilson, J.C., Bindschadler, R.A., 1992. Application of image cross-correlation to the measurement of glacier velocity using satellite image data. *Remote Sensing Environment* 42 (3), 177–186.
- Schäller, F., von Blanckenburg, Hovius, N., Kubik, P.W., 2001. Large-scale erosion rates from in situ-produced cosmogenic nuclides in European river sediments. *Earth and Planetary Science Letters* 188, 441–458.
- Searle, M.P., 1991. *The Geology and Tectonics of the Karakoram Mountains*. John Wiley and Sons, Chichester, UK. 358 pages.
- Searle, M.P., Rex, A.J., Tirrul, R., Rex, D.C., Barnicoat, A., 1989. Metamorphic, magmatic and tectonic evolution of the central Karakoram in the Biafo–Baltoro–Hushe regions of N. Pakistan. In: Malinconico, L.L., Lillie, R.S. (Eds.), *Geology and Tectonics of the Western Himalaya*. Geological Society of America Special Publication, vol. 232, pp. 47–73.
- Seong, Y.B., Owen, L.A., Bishop, M., Bush, A., Copeland, L., Finkel, R.C., Kamp, U., Shroder, J.F., 2007. Glacial history of the Central Karakoram. *Quaternary Science Reviews*, 26, 3384–3405.
- Seong, Y.B., Owen, L.A., Bishop, M.P., Bush, A., Clendon, P., Copland, P., Finkel, R., Kamp, U., Shroder, J.F., 2008. Rates of fluvial bedrock incision within an actively uplifting orogen: Central Karakoram Mountains, northern Pakistan. *Geomorphology* 97 (3–4), 274–286.
- Seong, Y.B., Owen, L., Yi, C., Finkel, R., Schoenbohm, L., 2009a. Geomorphology of anomalously high glaciated mountains at the northwestern end of Tibet: Muztag Ata and Kongur Shan. *Geomorphology* 103, 227–250.
- Seong, Y.B., Owen, L.A., Bishop, M.P., Bush, A., Clendon, P., Copland, P., Finkel, R., Kamp, U., Shroder, J.F., 2009b. Landforms and landscape evolution in the Skardu, Shigar and Braldu Valleys, Central Karakoram. *Geomorphology* 103, 251–267.
- Shroder Jr., J.F., 1993. Himalaya to the sea: geomorphology and the Quaternary of Pakistan in the regional context. In: Shroder Jr., J.F. (Ed.), *Himalaya to the Sea: Geology, Geomorphology, and the Quaternary*. Routledge Press, London, pp. 1–42.
- Shroder Jr., J.F., Bishop, M.P., 2004. Mountain geomorphic systems. In: Bishop, M.P., Shroder Jr., J.F. (Eds.), *Geographic Information Science and Mountain Geomorphology*. Springer-Praxis, London, UK.
- Shroder, J.F., Bishop, M.P., Copland, L., Sloan, V.F., 2000. Debris-covered glaciers and rock glaciers in the Nanga Parbat Himalaya, Pakistan. *Geografiska Annaler* 82A, 17–31.
- Small, E.E., Anderson, R.S., Repka, J.L., Finkel, R., 1997. Erosion rates of alpine bedrock summit surfaces deduced from in situ Be-10 and Al-26. *Earth and Planetary Science Letters* 150, 413–425.
- Stone, J.O., 1999. A consistent Be-10 production rate in quartz–muons and altitude scaling. *AMS-8 Proceedings Abstract Volume*, Vienna, Austria.
- Stone, J.O., 2000. Air pressure and cosmogenic isotope production. *Journal of Geophysical Research* 105, 23,753–23,759.
- Vance, D., Bickle, M., Ivy-Ochs, S., Kubik, P.W., 2003. Erosion and exhumation in the Himalaya from cosmogenic isotope inventories of river sediments. *Earth and Planetary Science Letters*, 206, 273–288.
- Visser, Ph.C., 1938. *Wissenschaftliche Ergebnisse der Niederländischen Expeditionen in den Karakorum und die Angrenzenden Gebiete in den Jahren 1922, 1925, 1929/30 und 1935: Band II, Glaziologie*. E.J. Brill, Leiden, Netherlands. 216 pages.
- Wake, C.P., 1989. Glaciochemical investigations as a tool for determining the spatial and seasonal variation of snow accumulation in the central Karakoram northern Pakistan. *Annals of Glaciology* 13, 279–284.
- Washburn, A.L., 1939. Karakorum glaciology. *American Journal of Science* 237, 138–146.
- Whalley, W.B., 1984. Rockfalls. In: Brunson, D., Prior, D.B. (Eds.), *Slope Instability*. Wiley, Chister, pp. 217–256.